

A Theoretical Study of the Structure and Thermochemical Properties of Alkali Metal Fluoroplumbates MPbF₃

A. I. Boltalin, Yu. M. Korenev, and V. A. Sipachev*

Faculty of Chemistry, Moscow State University, 119899 Moscow, Russia

Received: March 29, 2007; In Final Form: May 19, 2007

Molecular constants of MPbF₃ (M = Li, Na, K, Rb, and Cs) were calculated theoretically at the MP2(full) and B3LYP levels with the SDD (Pb, K, Rb, and Cs) and cc-aug-pVQZ (F, Li, and Na) basis sets to determine the thermochemical characteristics of the substances. Satisfactory agreement with experiment was obtained, including the unexpected nonmonotonic dependence of substance dissociation energies on the alkali metal atomic number. The bond lengths of the theoretical CsPbF₃ model were substantially elongated compared with experimental estimates, likely because of errors in both theoretical calculations and electron diffraction data processing.

1. Introduction

Thanks to their unique optical properties (low refractive indexes), metal fluorides are extensively used as antireflection and protective coatings. The preparation of such coatings by chemical vapor deposition (CVD) requires knowledge of the thermodynamic properties of gas-phase reaction participants and their temperature dependences. This in turn presupposes knowledge of the molecular constants of the substances, including structure characteristics and vibrational frequencies.

Unfortunately, these objects are difficult to study experimentally because of complex vapor compositions and a low intensity of vibrational bands, which are, in addition, situated in the far IR spectral range. We therefore deemed it worthwhile to undertake a quantum-chemical study of alkali metal fluoroplumbates MPbF₃ (M = Li, Na, K, Rb, and Cs) used in CVD processes, not least to gain experience in handling such systems.

Of all the MPbF₃ compounds, only the structure of CsPbF₃ was studied by gas-phase electron diffraction.^{1,2} The molecule was found to be a trigonal bipyramid, symmetry C_{3v}. Note that the thermodynamic characteristics calculated in refs 1 and 2 on the basis of the results obtained in these works and using certain model considerations were strongly at variance with the mass spectrometry data.^{3,4}

The IR spectra of matrix-isolated MPbF₃ were studied in ref 5. Only two comparatively high-frequency bands were, however, recorded.

The validity of our theoretical calculations was evaluated against the mass spectrometric data on the energies of MPbF₃ dissociation to MF and PbF₂ calculated according to the second and third laws of thermodynamics and from the ion appearance potentials.^{3,4}

2. Methodological Section

The main difficulty in handling such objects as alkali metal fluoroplumbates is the selection of basis sets, which should satisfy one important requirement: they should equally well describe the MF and PbF₂ moieties. Our final choice was as follows: aug-cc-pVQZ for F, Li, and Na and Stuttgart/Dresden

(SDD) or Stevens–Basch–Krauss (SBK) ECPs for the other elements. In global minimum structure, energy, and frequency calculations, the SDD basis sets were augmented by bits and pieces from other sources (diffuse (exponent 0.0168) and polarization (0.179) functions for Pb, diffuse (0.0047) and polarization @d (0.458 and 0.1145) and @f (1.11) functions for K, and polarization functions for Rb (0.24) and Cs (0.19)), which slightly improved agreement with the reliable experimental data on the system's constituents (PbF₂ and MF).^{6,7} In fact, simple SDD for Pb plus 6-311+G(d) for F was the best choice for PbF₂, but the 6-311+G(d) basis set for F gave unsatisfactory results for alkali metal fluorides.

The calculations were performed using the PC Gamess⁸ and Gaussian-03⁹ packages both at the MP2(full) level and with the B3LYP hybrid functional and its various modifications implemented in Gamess.

The transition states were sought starting from energy minimum geometries by applying first the QST2 procedure (Gaussian) with default and then QST3 with very tight optimization tolerance values. The intrinsic reaction coordinate calculations were performed using the Gamess package because the optimization criteria in the corresponding Gaussian procedure were too loose, whereas the potential energy surfaces of our systems were fairly flat. Population analyses of compounds with heavy atoms are impeded for several reasons, in particular, because of the unavailability of either the Merz–Kollman or Breneman radii.

Because chemical vapor deposition and matrix isolation experiments are often performed under harsh (e.g., target bombardment) conditions, we deemed it necessary to perform calculations not only for the ground but also for excited states of molecules. We were then largely interested in energy differences rather than exact molecular constant values. For this reason, these calculations were made with the 6-311+G(d,f) basis sets for fluorine and light alkali metal atoms. Our single-excitation configuration interaction (CIS) calculations of the lowest triplet and singlet excited states of the LiPbF₃ through CsPbF₃ complexes showed that excited-state contributions to thermodynamic functions could safely be ignored under usual conditions because of the high excitation energies. The results

* Corresponding author. E-mail: sipachev@online.ru

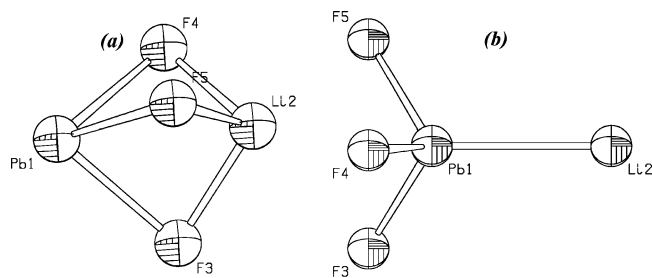


Figure 1. Structure of LiPbF₃ in the ground state: (a) global **GM1** and (b) local **GM2** minima.

obtained are nevertheless of certain phenomenological interest and likely have some bearing on practical matters.

All calculations were performed without symmetry restrictions.

3. Ground-State Geometry

The geometry of the alkali metal fluoroplumbate molecules is almost obvious. In all probability, they should form trigonal bipyramids of C_{3v} symmetry with Pb and M in bipyramid vertices and fluorine atoms in the equatorial plane (Figure 1a); this expectation is in agreement with the earlier ED^{1,2} and spectral⁵ data. Our calculation results show that MPbF₃ do indeed have trigonal pyramidal structures, but not exactly regular. One of the M–F and Pb–F bonds is slightly different from the other two in all alkali metal fluoroplumbates (Table 1). Although the difference is insignificant, it is persistently reproduced for all MPbF₃ at all levels of calculations. The exact point symmetry group of the molecules is therefore C_s .

Symmetry lowering can be caused by an admixture of the **TS2** structure (see below). Note that the difference between the Pb–F and M–F bond lengths disappears in the **GM2** and saddle structures (Table 1), whose symmetry is exactly C_{3v} .

However, in reality, the potential energy surface of the ground state is not all that simple. We were able to locate at least four more stationary points.

For MPbF₃, this surface has a ravine along the coordinate corresponding to simultaneous equal changes in the M–Pb–F angles. (The MPbF@3 “umbrella” becomes turned inside out along this coordinate.) The corresponding energy profile is plotted in Figure 2 for LiPbF₃. The deeper (global) minimum (**GM1**) relates to the configuration shown in Figure 1a, and the shallower (local) one (**GM2**), to the configuration shown in Figure 1b. The parameters of these two configurations and the saddle point are listed in Table 1.

A decrease in the charge on Li in the configuration with the PbF₃ pyramid turned toward the Li atom by its Pb vertex is evidence that this structure contains a covalent Pb–Li bond. According to Mulliken population analysis, the Li–Pb bond order is 0.612 in this configuration. The local energy minimum (**GM2**) is raised by 0.15423 au (~405 kJ/mol) above the global minimum, and the structure shown in Figure 1b can hardly contribute much to the properties of LiPbF₃ under the conditions of usual electron diffraction, mass spectrometric, and CVD experiments (600–800 K).

GM1 and **GM2** are separated by a saddle point of order 3. Its imaginary frequencies correspond to totally symmetrical and doubly degenerate M–Pb–F bending vibrations. At the saddle point, the geometry of the PbF₃ moiety is almost planar ($\angle\text{Li–Pb–F} \approx 88^\circ$).

For heavier alkali metal atoms, the shape of the potential energy curve along the $\angle\text{M–Pb–F}$ coordinate is closely similar to that shown in Figure 2, but the local minimum transforms

into a transition state (**TS1**, one imaginary frequency 16.7i cm^{-1}). Graphically, the transition-state geometry is indistinguishable from that shown in Figure 1b. Its imaginary frequency corresponds to the doubly degenerate F–Pb–M bending mode. (The corresponding (real) frequency of LiPbF₃ in the **GM2** state is about 50 cm^{-1} .) The M–Pb bond order decreases rapidly as the atomic number of M increases, to 0.414 for Na–Pb and 0.062 for Cs–Pb. The IRC path from this transition state, which leads to the global minimum, is fairly long; several intermediate structures are shown schematically in Figure 3.

There is one more saddle point of order 1 (one imaginary frequency) on the ground-state potential energy surface outside the section shown in Figure 2. The corresponding structure (Table 1, **TS2**, one imaginary frequency 91.4i cm^{-1}) is almost strictly planar and is graphically indistinguishable from that shown in Figure 6 for the triplet excited state (**TM1**), although its Pb–F bond lengths are strongly elongated compared with the triplet-state geometry (Table 1). Conversely, the M–F bonds are shortened somewhat. For CsPbF₃, the **TS2** energy is 0.0541349 au (~142.02 kJ/mol) counting from the global minimum level, that is, the relative energy of **TS2** increases from LiPbF₃ through CsPbF₃. The imaginary frequency can be described as the folding of the planar structure (Figure 6) about the F3F5 axis above or below the F3PbF5 plane. Simultaneously, the M2 and F4 atoms move toward each other. Forward and back IRC paths lead to the same ground-state global minimum configuration (Figure 1a).

The IRC paths through **TS1** and **TS2** that begin and end at the global minimum configuration change the orientation of the symmetry plane in MPbF₃, which may pass through any of the three fluorine atoms.

In addition, LiPbF₃ molecules form dimers in the gas phase (Table 1, Figure 4). The dimer has C_s symmetry, and its symmetry plane contains the Pb1, Pb2, Li3, Li4, F8, and F10 atoms. Two LiPbF₃ moieties in it are largely held together by Coulomb interactions; in any event, the Pb2–F10 bond order is lowered two times compared with the other Pb–F bonds. The geometry of the dimer is also determined by Pb1⋯F5 and Pb1⋯F9 purely Coulomb interactions (the Pb1⋯F5 and Pb1⋯F9 bond orders are less than 0.05). All the Li3–F_{bridge} (F_{bridge} = F10, F9, and F5) bonds are elongated equally compared with the other Li–F distances. The dissociation energy of the dimer into two monomers is –271.26 kJ/mol; the dimer therefore cannot be present in the gas phase in noticeable amounts under the conditions specified above (600–800 K). Its characteristics are listed in Table 1 (bond lengths and charges are averaged over two LiPbF₃ moieties). Heavier alkali metal derivatives behave similarly to the lithium compound.

4. Excited-State Geometries

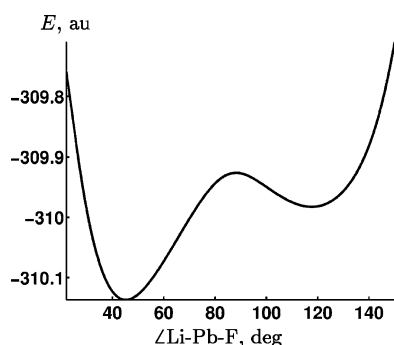
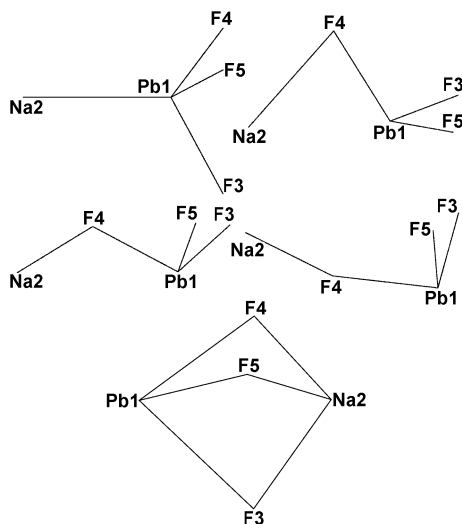
In the singlet excited state, MPbF₃ virtually dissociates into two neutral species, PbF₃ and M (Table 1). Naturally, the potential energy profile along the $\angle\text{M–Pb–F}$ coordinate contains two dips of approximately equal depths (Table 1, **SM1** and **SM2**) situated symmetrically with respect to the planar ($\angle\text{M–Pb–F} = 90^\circ$) configuration of the PbF₃ moiety (Figure 5). The potential energy minimum of the singlet excited state is raised above the global ground-state minimum by 0.2775 au (~7.5452 eV), the vertical excitation energy being 9.7052 eV. The spins (antiparallel) are largely localized on Li and Pb (1.0 and 0.724, respectively).

Certainly, residual Li–Pb interaction at $\angle\text{Li–Pb–F} = 114.1^\circ$ (charge on Li +0.145) is a calculational artifact: optimization stops at $r(\text{Li–Pb}) = 10.048 \text{ \AA}$ because the potential energy

TABLE 1: Mean Bond Lengths and Charges in Li–F–Pb Species (DFT Calculations, B3LYP Functional)

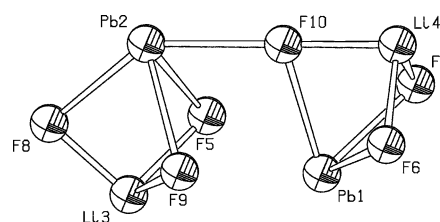
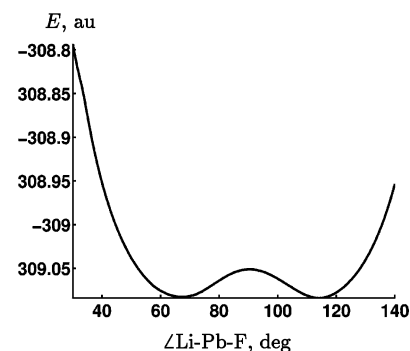
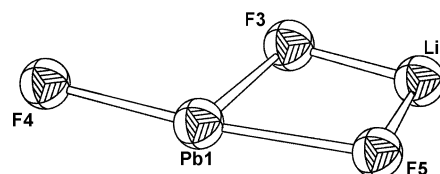
stationary point	energy ^a	internuclear distances				Mulliken charges			
		Pb–F	Li–F	Pb–Li	PbF ^b	LiF ^b	Pb	F	Li
LiPbF ₃ , ground state									
GM1 ^c	0.0	2.161	1.873	2.591	2.159	1.877	+1.132	−0.635	+0.772
GM2 (TS1) ^d	0.1542	2.048	4.073	2.696			+1.485	−0.678	+0.549
saddle	0.2104	2.153	3.401	2.709			+1.381	−0.717	+0.769
TS2	0.0339	2.366	1.715	3.042	2.103	4.537	+1.051	−0.534	+0.549
LiPbF ₃ , singlet excited state									
SM1 ^e	0.2763	1.998	1.018	0.048			+1.727	−0.624	+0.145
SM2 ^f	0.2775	1.981	0.497	1.094			+1.821	−0.606	−0.004
saddle	0.3091	2.104	8.828	8.610			+1.774	−0.706	+0.215
LiPbF ₃ , triplet excited state									
TM1	0.1753	2.203	1.739	2.962	2.048	4.610	+1.376	−0.706	+0.741
TM2	0.2124	2.092	1.955	2.673	2.258	1.765	+1.302	−0.682	+0.745
TS3	0.2185	2.071	4.130	3.835	2.222	1.612	+1.389	−0.727	+0.792
TS4	0.2131	2.196	1.788	2.746	2.050	2.344	+1.306	−0.681	+0.739
(LiPbF ₃) ₂ , dimer									
minimum	0.0517 ^g	2.221	1.798	2.679	2.301	1.904	+1.094	−0.533	+0.504

^a The energies (au) are counted from the ground-state global minimum. ^b Unique fluorine atom. The other two Pb–F and Li–F bonds are strictly or approximately equal. ^c Global minimum, $\angle\text{Li–Pb–F} = 45.0^\circ$. ^d Local minimum, $\angle\text{Li–Pb–F} = 117.7^\circ$; transforms into transition state **TS1** for $M = \text{Na}$ through Cs . ^e $\angle\text{Li–Pb–F} = 114.1^\circ$. ^f $\angle\text{Li–Pb–F} = 67.5^\circ$. ^g $E_{(\text{LiF}_3)_2/2} - E_{\text{LiPbF}_3}$.

**Figure 2.** Potential energy profile along the $\angle\text{Li–Pb–F}$ coordinate.**Figure 3.** Several structures along the intrinsic reaction coordinate path from **TS2** to the global minimum geometry.

surface along this coordinate becomes too flat and the gradient, too low, rather than because a minimum is attained.

In the triplet excited state, the potential energy surface has a ridge rather than ravine along the $\angle\text{M–Pb–F}$ coordinate. The equilibrium configuration of MPbF_3 in this state is quite different from those found for the ground and singlet excited states (Table 1, Figure 6, **TM1**), and its energy is only 0.1753 au (~ 460 kJ/mol) higher compared with the ground state, the vertical excitation energy being 7.7530 eV. For CsPbF_3 , the energy

**Figure 4.** Structure of $(\text{LiPbF}_3)_2$.**Figure 5.** Potential energy profile of LiPbF_3 in the singlet excited state.**Figure 6.** Structure of LiPbF_3 in the triplet excited state (Table 1, **TM1**).

difference between the triplet excited and ground states is $0.1709\text{au} \approx 448$ kJ/mol, which is slightly lower than for LiPbF_3 . Some characteristics of the molecule in the triplet excited state are listed in Table 1 (**TM1**).

Here, the lead atom has a T-shaped configuration, and the molecule as a whole is strictly planar (C_s symmetry). The charges on the atoms are therefore close to those obtained for the saddle point (planar PF_3 group) ground-state configuration. The spins are largely localized on Pb (1.787), which is quite natural, because the other atoms have either almost full (F) or

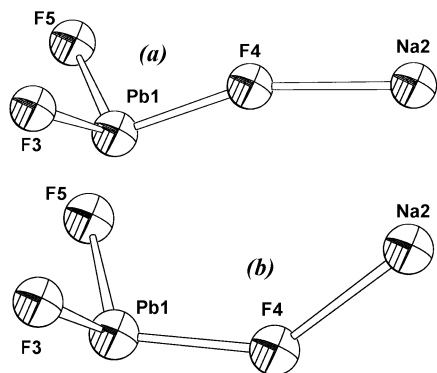


Figure 7. Structure of NaPbF₃ in the triplet excited state: (a) local minimum **TM3** and (b) transition state **TS5**.

almost empty (M) outer shells. Naturally, there exists an equivalent structure with M attached to the F3 and F4 atoms.

All MPbF₃ molecules have a secondary minimum in the triplet excited state (Table 1, **TM2**), which corresponds to a strongly distorted trigonal bipyramid (*C_s* symmetry). The differences between both the Pb–F and Li–F bond lengths are as large as ~ 0.2 Å in this structure. The transition state between **TM1** and **TM2** (**TS4**, one imaginary frequency 146.2i cm⁻¹) also has a trigonal bipyramidal geometry distorted to a still greater extent. One of its Li–F bonds is longer by as much as ~ 0.6 Å than the other two (this bond disappears in the structure corresponding to **TM1**). Two equal bonds are considerably (by ~ 0.2 Å) shorter than in the structure corresponding to **TM2** and slightly (by ~ 0.05 Å) longer than in the structure corresponding to **TM1**.

The behavior of LiPbF₃ in the triplet excited state differs strongly from that of the heavier alkali metal derivatives. The transition state (Table 1, **TS3**, one imaginary frequency 89.1i cm⁻¹) between two equivalent structures with Li attached to the F3 and F5 or F3 and F4 atoms is strictly planar, and the Pb1–F3–Li2 angle is 180°. Interestingly, the structure remains planar along the whole IRC path connecting two minima and passing through **TS3**.

Heavier alkali metal fluoroplumbates have an additional minimum with a single F atom involved in bonding with M and a flattened pyramidal PbF₃ configuration. This minimum is raised by 151.93 kJ/mol above **TM1** (Figure 7a, **TM3**, the lowest frequency at 32.3 cm⁻¹ corresponds to Pb1–F4–Na2 bending vibrations). Interestingly, the charge on Na in both **TM3** and **TS5** (see below) is close to zero, and the spins are localized on Na (~ 1.011) and Pb (~ 0.773) (the charge on Li in **TS3** is +0.792). The energy of the transition state (Figure 7b, **TS5**, one imaginary frequency 90.3i cm⁻¹; like the lowest **TM3** frequency, it corresponds to Pb1–F4–Na2 bending vibrations) between **TM1** and **TM3** (Figure 7a) is slightly higher and equals 158.47 kJ/mol. The F4–M bond in **TS5** is bent inside the PbF₃ pyramid, whereas, in the intermediate minimum (**TM3**), it is bent outward and at a smaller Pb1–F4–M angle.

Interestingly, along the IRC path from **TS5** to **TM1**, the Pb1–F4–M angle first narrows from $\sim 136^\circ$ to $\sim 108^\circ$, while the dihedral angles between the Pb1F4M2 and Pb1F4F5 and between the Pb1F4M2 and Pb1F4F3 planes, which are equal in **TS5**, remain unchanged. Next, the Pb1F4M2 fragment begins to rotate about the Pb1F4 axis toward the F5 or F3 atom (Figure 7), while the Pb1–F4–M2 angle changes very slowly and insignificantly. In the final configuration, this angle becomes $\sim 101^\circ$.

5. Discussion

The experimental data mentioned in section 2 are not very reliable (except the thermodynamic values determined mass

TABLE 2: Calculated (DFT, B3LYP) and Experimental^{1,2,5} Interatomic Distances (r_g , Å), Root-Mean-Square Amplitudes (l , Å), and Vibrational Frequencies (cm⁻¹) for CsPbF₃

parameter	calcd	exptl	parameter	calcd	exptl
r_g (Pb–F)	2.165	2.142(5)	l (Pb–F)	0.064	0.088(5)
r_g (Cs–F)	2.951	2.779(9)	l (Cs–F)	0.144	0.221(22)
r_g (F⋯F)	2.964	2.800(13)	l (F⋯F)	0.127	0.163(38)
r_g (Cs⋯Pb)	3.706	3.654(7)	l (Cs⋯Pb)	0.085	0.152(5)
$\nu(A_1)$ (CsPbF ₃)	457.8	456.0	$\nu(E)$ (CsPbF ₃)	416.5	405.0

TABLE 3: Calculated and Experimental Characteristics of MPbF₃ → MF + PbF₂ Reactions (kJ/mol)^a

reaction	energy (calcd)	enthalpy (calcd)	energy (AP)	enthalpy	
				III law	II law
LiPbF ₃ = LiF + PbF ₂	213.18	209.83	238(30)	225.8(8.4)	219.0(2.4)
NaPbF ₃ = NaF + PbF ₂	241.63	237.62	252(30)	252.0(8.4)	257.9(4.0)
KPbF ₃ = KF + PbF ₂	255.80	245.05	250(30)	262.5(11.0)	
RbPbF ₃ = RbF + PbF ₂	235.79	229.60	200(30)	229.8(11.4)	
CsPbF ₃ = CsF + PbF ₂	216.66	210.12	205(30)	212.2(12.6)	

^a The enthalpy values for M = Li, Na, K, Rb, and Cs correspond to 799, 714, 800, 800, and 800 K, respectively. The second and third columns contain values calculated in this work from quantum-chemical data (corrected for zero-point energies), the “AP” column contains values calculated from ion appearance potentials,^{3,4} and the “III law” and “II law” columns, values calculated by the third and second laws of thermodynamics, respectively, from the mass spectrometric data.^{3,4}

spectrometrically). Indeed, the ED structure of CsPbF₃ was refined in refs 1 and 2 using an empirical force field, which very poorly reproduced the thermodynamic properties of this compound. The IR spectra obtained in ref 5 were not corrected for the matrix effect. The results reported in refs 1, 2, and 5 are compared with our theoretical data on CsPbF₃ in Table 2.

The r_g (calculated) values are the quantum-chemical geometric parameters corrected for vibrational (including anharmonic) effects according to ref 10 (the Shrink program). We see that the experimental electron diffraction structure^{1,2} (Table 2) is noticeably contracted compared with that obtained in quantum-chemical calculations. Conversely, the amplitudes reported in refs 1 and 2 are appreciably exaggerated. These discrepancies might appear because, first, quantum-mechanical calculations poorly reproduce M–F distances with larger M atoms and, second, the authors of refs 1 and 2 used an empirical force field constructed by fitting the theoretical $sM(s)$ curve to experimental. This approach can hardly be considered reliable. In any event, the low frequencies obtained in refs 1 and 2 (67.3 cm⁻¹, $(\nu + \delta)(\text{CsF}_3)$) were underestimated by ~ 40 cm⁻¹ compared with our theoretical results (107–120 cm⁻¹). The corresponding frequency factors (and, accordingly, the amplitudes) were therefore strongly exaggerated (below 100 cm⁻¹, the frequency factor increases exponentially as the frequency decreases). The use of too large amplitude values in the refinement of electron diffraction data might in turn cause errors in structure parameter estimates.

The experimental and theoretical frequency values closely agree with each other. It should, however, be borne in mind that the experimental frequencies contain unknown matrix shifts.

The thermodynamic characteristics of MPbF₃ were obtained in the rigid rotator–harmonic oscillator approximation with corrections for zero-point energies. A comparison of our data with those reported in refs 3 and 4 is given in Table 3.

The remarkable feature of these results is nonmonotonic variations in $\Delta_{\text{diss}}H$ along the series of alkali metal fluoroplumbates. We were unable to reproduce this trend with basis sets smaller than those used in the present work (Figure 8).

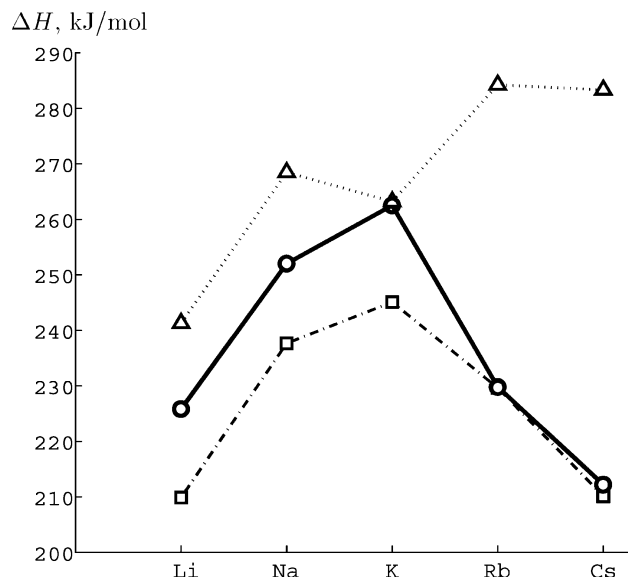


Figure 8. Enthalpies of dissociation of MPbF_3 : experimental (thick line, circles), calculated using the aug-cc-pVQZ basis set for F (dot-and-dash line, squares), and calculated using the 6-311+G(d) basis set for F (dotted line, triangles).

Conversely, the bond lengths and vibrational frequencies change monotonically along the series of alkali metals. The Pb–F bond length decreases from 2.161 (LiPbF₃) to 2.152, 2.147, 2.146, and 2.145 Å in Na, K, Rb, and Cs derivatives, respectively, without noticeable anomalies, most sharply in passing from Li to Na and very insignificantly over the last members of the series. In contrast, the M–F length increases (almost linearly) from Li to Cs. The highest vibrational frequency changes in the order Li \gg Na \approx K \approx Rb \approx Cs; that is, starting with K⁺, cations weakly influence the characteristics of the PbF₃ pyramid.

These data lead us to suggest that the PbF₃ moiety has a fairly strained geometry in the lithium compound and virtually fully relaxes in passing to KPbF₃. We can assume, as a very crude approximation, that the strain energy in the Coulomb field of a singly charged cation is zero in the potassium derivative, and the strain energies stored in LiPbF₃ and NaPbF₃, which contribute to the ease of the dissociation of these species, can be counted from this level. We therefore calculated the energies of the PF₃ unit with the geometries corresponding to **GM1** for LiPbF₃ (E_{Li}), NaPbF₃ (E_{Na}), and KPbF₃ (E_{K}) (for Rb and Cs, these energies are approximately the same as for the potassium derivative) and added the $E_{\text{Li}} - E_{\text{K}}$ and $E_{\text{Na}} - E_{\text{K}}$ differences to the enthalpies of dissociation of the lithium and sodium derivatives. The enthalpies of dissociation corrected for the strain energies of the PbF₃ moiety this way became 265.35, 253.91, 245.05, 229.60, and 210.12 kJ/mol for M = Li, Na, K, Rb, and Cs, respectively. This is a series that can more naturally be expected for alkali metal derivatives. The dissociation energy is then a linear function of the atomic number of M ($\Delta_{\text{diss}}H$, kJ/mol $\approx 268 - 1.1N \pm 2.5$, where N is the atomic number).

6. Conclusions

Fluorine derivatives, especially inorganic fluorides, are difficult objects for quantum-chemical studies. Nevertheless, our

approach to the problem (the main point was the selection of the basis set for F that equally well described the two moieties constituting the molecules) allowed us to reproduce the most reliable experimental results. Figure 8 shows that basis set selection is crucial to the description of the thermochemical characteristics of the systems studied in this work and, probably, related systems. The theoretical $\Delta_{\text{diss}}H$ values for M = Li, Na, and K are slightly underestimated, but the general trend is reproduced fairly well, Li < Na < K > Rb > Cs. This allows us to claim the validity of our quantum-chemical data.

The results described above show that the shape of MPbF₃ potential energy surfaces is fairly complex. Various structures can therefore be formed under harsh (e.g., target bombardment) conditions frequently used in CVD and matrix isolation experiments. Moreover, these structures can be quenched in the solid state because of barriers to interconversions. The problem of the structural homogeneity of coatings obtained this way should therefore be given special attention.

The molecular constants of MPbF₃ determined in this work were used to calculate the temperature dependences of the thermodynamic functions of MPbF₃ required for practical applications, including excited-state functions and characteristics of reactions with the participation of MPbF₃. These results will be published elsewhere.

References and Notes

- (1) Demidov, A. V.; Ivanov, A. A.; Zazorin, E. Z.; Rezanova, D. A.; Spiridonov, V. P.; Moroz, A. E. *Zh. Fiz. Khim.* **1992**, *66*, 1532–1536.
- (2) Lyutsarev, V. S.; Lobanov, V. S.; Spiridonov, V. P. *Zh. Fiz. Khim.* **1993**, *67*, 975–978.
- (3) Boltalin, A. I.; Rykov, A. N.; Korenev, Yu. M. *Zh. Neorg. Khim.* **1989**, *34*, 2398–2403.
- (4) Boltalin, A. I.; Rykov, A. N.; Korenev, Yu. M. *Zh. Neorg. Khim.* **1990**, *35*, 2908–2912.
- (5) Ault, B. S. *J. Chem. Phys.* **1981**, *85*, 3083–3087.
- (6) Huber, K. P.; Herzberg, G. *Molecular Spectra and Molecular Structure. IV. Constants of Diatomic Molecules*; Van Nostrand: New York, 1979.
- (7) Hauge, R. H.; Hastie, J. W.; Margrave, J. L. *J. Mol. Spectrosc.* **1973**, *45*, 420–426.
- (8) Granovskii, A. A. *PC GAMESS*, version 7.0. <http://classic-chem.msu.su/gran/gameess/index.html>.
- (9) Frisch, M. J.; Trucks, G. W.; Schlegel, H. B.; Scuseria, G. E.; Robb, M. A.; Cheeseman, J. R.; Montgomery, J. A., Jr.; Vreven, T.; Kudin, K. N.; Burant, J. C.; Millam, J. M.; Iyengar, S. S.; Tomasi, J.; Barone, V.; Mennucci, B.; Cossi, M.; Scalmani, G.; Rega, N.; Petersson, G. A.; Nakatsuji, H.; Hada, M.; Ehara, M.; Toyota, K.; Fukuda, R.; Hasegawa, J.; Ishida, M.; Nakajima, T.; Honda, Y.; Kitao, O.; Nakai, H.; Klene, M.; Li, X.; Knox, J. E.; Hratchian, H. P.; Cross, J. B.; Adamo, C.; Jaramillo, J.; Gomperts, R.; Stratmann, R. E.; Yazyev, O.; Austin, A. J.; Cammi, R.; Pomelli, C.; Ochterski, J. W.; Ayala, P. Y.; Morokuma, K.; Voth, G. A.; Salvador, P.; Dannenberg, J. J.; Zakrzewski, V. G.; Dapprich, S.; Daniels, A. D.; Strain, M. C.; Farkas, O.; Malick, D. K.; Rabuck, A. D.; Raghavachari, K.; Foresman, J. B.; Ortiz, J. V.; Cui, Q.; Baboul, A. G.; Clifford, S.; Cioslowski, J.; Stefanov, B. B.; Liu, G.; Liashenko, A.; Piskorz, P.; Komaromi, I.; Martin, R. L.; Fox, D. J.; Keith, T.; Al-Laham, M. A.; Peng, C. Y.; Nanayakkara, A.; Challacombe, M.; Gill, P. M. W.; Johnson, B.; Chen, W.; Wong, M. W.; Gonzalez, C.; Pople, J. A.; Gaussian, Inc.: Pittsburgh PA, 2003.
- (10) Sipachev, V. A. In *Advances in Molecular Structure Research*, vol. 5; Hargittai, I., Hargittai, M., Eds.; JAI: Greenwich, 1999; pp 263–311. Sipachev, V. A. *J. Mol. Struct.* **2001**, *567–568*, 67–72. Sipachev, V. A. *J. Mol. Struct.* **2004**, *693*, 235–240. Sipachev, V. A. In *Strength from Weakness: Structural Consequences of Weak Interactions in Molecules, Supermolecules, and Crystals*; Domenicano, A., Hargittai, I., Eds.; Kluwer: Dordrecht, 2002; pp 73–90.